The Local Environment of Cu^+ in Cu−Y Zeolite and Its Relationship to the Synthesis of Dimethyl Carbonate

Ian J. Drake,[†] Yihua Zhang,[†] Daniel Briggs,[†] Bomyi Lim,[†] Tanguy Chau,[†] and Alexis T. Bell*[,†,‡]

Department of Chemical Engineering, University of California, Berkeley, California 94720-1462, Chemical Sciences Division, Lawrence Berkeley National Laboratory, 1 Cyclotron Road, Berkeley, California 94720

Received: September 2, 2005

Cu-exchanged Y zeolite was investigated in order to determine the location of the copper cations relative to the zeolite framework and to determine which Cu cations are active for the oxidative carbonylation of methanol to dimethyl carbonate (DMC). Cu−Y zeolite was prepared by vapor-phase exchange of H−Y with CuCl. The oxidation state, local coordination, and bond distances of Al and Cu were determined using Al K-edge and Cu K-edge X-ray absorption spectroscopy (XAS). Complimentary information was obtained by H_2 temperature-programmed reduction and by in-situ infrared spectroscopy. Cu−Y has a Cu/Al ratio of unity and very little occluded CuCl. The average Al−O and Al−Cu bond distances are 1.67 Å and 2.79 Å, respectively, and the average Cu−O and Cu−Si(Al) bond distances are 1.99 Å and 3.13 Å, respectively. All of the Cu exchanged is present as Cu^+ in sites I′, II, and III′. Cu−Y is active for the oxidative carbonylation of methanol, and at low reactant contact time produces DMC as the primary product. With increasing reactant contact time, DMC formation decreases in preference to the formation of dimethoxy methane (DMM) and methylformate (MF). The formation of DMM and MF is attributed to the hydrogenation of DMC and the hydrogenolysis of DMM, respectively. Observation of the catalyst under reaction conditions reveals that most of the copper cations remain as Cu^+, but some oxidation of Cu^+ to Cu^{2+} does occur. It is also concluded that only those copper cations present in site II and III′ positions are accessible to the reactants, and hence are catalytically active. The dominant adsorbed species on the surface are methoxy groups, and adsorbed CO is present as a minority species. The relationship of these observations to the kinetics of DMC synthesis is discussed.

1. Introduction

Cu−USY and Cu−X zeolites have previously been shown to be effective catalysts for the synthesis of dimethyl carbonate (DMC) and dimethoxy methane (DMM).[1−3] Both products are of commercial interest, since DMC might serve as a replacement for MTBE in gasoline and DMM is a clean-burning synthetic diesel fuel.[4] While the literature describes many methods for the introduction of Cu into faujasite,[5−8] little is known about the local environment of the Cu cations and the relationship of the cation siting to DMC catalyst activity and selectivity.[1−3]

Faujasite (the framework structure common to zeolites X, Y, and USY) has three general cation-exchange sites that can be occupied by Cu. These sites are referred to commonly as site I(I′), site II(II′), and site III(III′) and are illustrated in Figure 1.[9] Rietveld refinement of XRD data for Cu−Y suggests that only the I′ and II positions are occupied when the catalyst is prepared by vapor phase exchange of NH_4^+−Y with CuCl to obtain a final Cu/Al ratio of 0.8, and EXAFS data support the occupancy fraction determined from XRD analysis.[8] While site III′(III) was not found to be occupied in this study, investigations of Cu−Y prepared by aqueous exchange with either $CuCl_2$ or $Cu(NO_3)_2$ and subsequent reduction of Cu^{2+} to Cu^+ in H_2 did

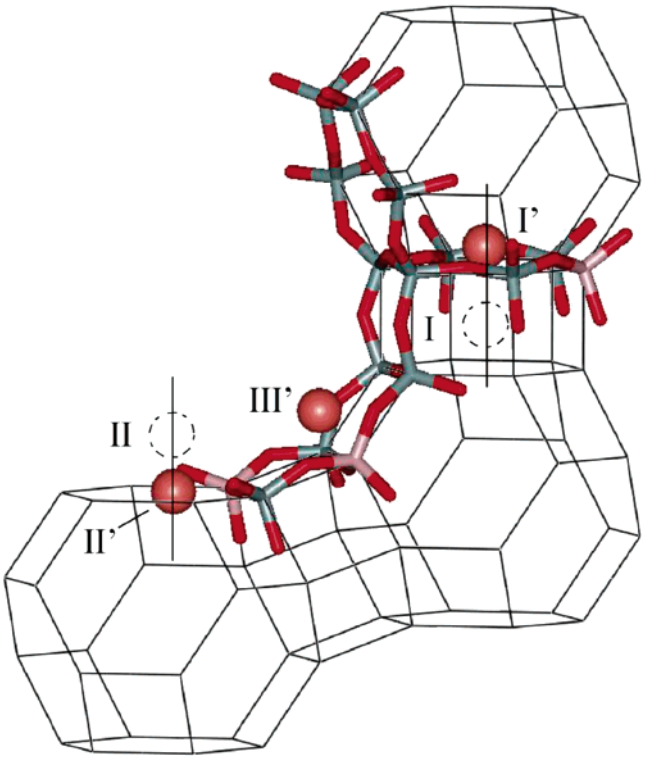

Figure 1. Possible locations for Cu^+ in faujasite.

* To whom correspondence should be addressed. Tel: 510-642-1536. Fax: 510-642-4778. E-mail: bell@cchem.berkeley.edu.
† University of California.
‡ Lawrence Berkeley National Laboratory.

10.1021/jp058245r CCC: $33.50
Published on Web 05/28/2006

result in the occupation of this site by Cu^+.[10−12] Cations in site III are the most accessible to reactants and have been suggested as the active site for NO_x reduction by NH_3.[13,14]

The objectives of this work were to determine the site distribution and local structure of Cu^+ cations in Y zeolite and to assess which types of Cu sites are active for DMC synthesis. Cu K-edge and Al K-edge XANES and EXAFS were used to characterize the local coordination and bond distance for Cu and Al atoms at the cation-exchange sites. Density functional theory (DFT) was used to predict the positions of Cu^+ cations located in sites I′, II, and III′, so that comparisons could be made with the experimental data. Cu site distribution was inferred from H_2 temperature-programmed reduction (TPR) experiments. DMC synthesis was carried out over a range of temperatures and feed residence times, and in-situ Cu K-edge XANES and infrared spectra were acquired in order to assess the effects of reaction conditions on the local environment of the active Cu^+ centers.

2. Experimental Section

2.1. Catalyst Preparation. 5.0 g of NH_4Na−Y (Strem Co., 5.0 wt % Na) was exchanged five times with 1 M NH_4Cl (5.0 g/L) in order to completely exchange Na^+ for NH_4^+ cations. Each exchange was performed at 363 K for 12 h. Following exchange, the material was washed with excess deionized water to remove Cl^- anions. The absence of Cl^- in the water was indicated by the absence of a white AgCl precipitate upon addition of $AgNO_3$. The material was dried under vacuum overnight followed by 12 h at 363 K. The dried material was then placed in a shallow bed within a quartz reactor (zeolite height = 5 mm, diameter of bed = 20 mm) and converted to H−Y by heating in flowing He (50 cm^3 min^{-1}). The temperature of the sample was first raised from 298 to 573 K at 5 K min^{-1}, and then raised from 573 to 723 K at 1 K min^{-1} before being held constant at 723 K for 6 h. The sample was then heated from 723 to 923 K at 1 K min^{-1} before being held at a constant temperature of 923 K for an additional 10 h. The freshly prepared H−Y was stored in a N_2 drybox, since it is highly air-sensitive. Cu^+-exchanged Y zeolite was prepared by mixing 500 mg of the dry H−Y with enough CuCl (mp = 703 K) to make a physical mixture containing Cu/Al = 1.1. The initial mixture was ground with a mortar and pestle within a drybox in order to achieve an intimate mixture of the two solids. The ground zeolite/CuCl mixture was then loaded into a quartz reactor introduced into the N_2-purged drybox. The reactor was sealed, transferred from the drybox, and connected to a flow manifold. The zeolite/CuCl mixture was heated to 923 K at 1 K min^{-1} in He flowing at 50 cm^3 min^{-1}. The exchange temperature was held isothermal at 923 K for 15 h. The as-prepared material had a yellow/tan color and was stored in an N_2-purged drybox until further use. The Cu, Al, Na, and Cl content of the catalyst was determined by Galbraith Laboratories (Knoxville, TN) using inductively coupled plasma (ICP) analysis. The zeolite structure was characterized by X-ray diffraction using a Siemens D5000 spectrometer. This instrument uses Cu−Kα radiation and a graphite monochromator, which also serves to remove the effects of Cu−Kβ radiation. The width of primary and receiving slits were adjusted to achieve optimum peak resolution.

2.2. ^{27}Al MAS NMR. Samples of NH_4-, H-, and Cu-exchanged Y were stored overnight in a closed volume containing a small amount of 1 M NH_4NO_3(aq) in order to equilibrate them with a fixed partial pressure of water (1.97 kPa at 298 K). Typically, 40−70 mg of zeolite was loaded into a 4 mm diameter zirconia rotor and sealed with a Kel-F cap. The ^{27}Al MAS NMR spectra were collected using a Bruker 500 (11.7 T) spectrometer equipped with a 4 mm MAS probe. The ^{27}Al signal was referenced to an aqueous solution of $Al(NO_3)_3$, which was also used to calibrate the 90° flip for nonselective irradiation of all aluminum transitions. The ^{27}Al MAS NMR spectra of all zeolite samples were acquired using a 15° flip angle; 2000 scans were accumulated using a 1 s pulse delay. The MAS spinning speed was 12.0 kHz.

2.3 X-ray Absorption Spectroscopy (XAS). *2.3.1 Cu K-edge.* EXAFS and XANES measurements were performed at the Stanford Synchrotron Radiation Laboratory (SSRL) on beamline 2−3, which was equipped with a Si (111) double crystal monochromator. The pre-monochromator vertical aperture of the beams was set to 0.5 mm for improved resolution, defining an energy resolution of 1.8 eV. The monochromator was detuned 20−30% at 400 eV above the Cu K-edge to attenuate the flux from higher order Bragg diffractions. Cu metal foil (7 μm) was used for energy calibration and changes in beam alignment.

Each sample was pressed into a rectangular pellet (0.43 × 1.86 cm, with the thickness dependent upon the amount of sample used) and loaded into an in-situ cell for transmission experiments.[15] Sufficient quantity of each sample was used (typically 5−10 mg for standards and 20−40 mg for samples) to give a calculated optical density ($\mu_m \rho x$) of 2.[16] Intensities of the beam were measured over a 900 eV range using a sampling step of 5 eV in the pre-edge and 0.3 eV in the XANES region (−30 to 30 eV relative to E_0) with a 1 s hold at each step. The EXAFS region was acquired for values of the wave vector (k) in 0.05 Å^{-1} steps for k = 1.78 Å^{-1} to 12 Å^{-1} and in 0.07 Å^{-1} steps for k = 12 Å^{-1} to 16 Å^{-1}, using holding times of 2 s and 3 s, respectively, in the two regimes. Ionization chambers (N_2 filled) were used to measure the incident and sample transmitted fluxes. A third detector was used to measure the flux through a (7 μm thick) Cu foil internal standard. Three to five scans were taken per sample to improve the signal-to-noise ratio.

A portable flow manifold was used to treat each material during XAS measurements. Each sample was first treated in He (99.999%) flowing at 60 cm^3 min^{-1}. An Omega CN2250 temperature controller was used to ramp the temperature at 10 K min^{-1} to 673 K. Following characterization by XAS, each sample was cooled to 298 K before exposure to a particular gas or mix. In separate experiments, pretreated Cu−Y was exposed to a mixture of He/CH_3OH, He/CO, or He/CO/O_2/CH_3-OH. Methanol vapor was introduced by saturating a particular gas with a tube containing methanol liquid at 298 K. The sample temperature was raised at 10 K min^{-1} to 403 K and then held at this temperature for 1 h. All XAS measurements were made during treatment.

2.3.2 Al K-Edge. Al K-edge EXAFS and XANES data were acquired at the Advance Light Source (ALS) at the Lawerence Berkeley National Laboratory (LBNL) on beamline 6.3.1.[17] This is a bending magnet beamline equipped with focusing optics and a Hettrick−Underwood-type varied-line-space (VLS) grating monochromator, which has a useable energy range between 200 and 2100 eV.[17] The grating monochromator (2400 l/mm) defined an energy resolution of $\Delta E/E$ = 5000. The pre-monochromator vertical aperture of the beam was set to 10 μm for optimal flux and resolution. The beam size at the sample was approximately 100 × 40 μm. Higher harmonics were not detected because the flux drops precipitously above 2100 eV. The ALS ring was operated at 1.9 GeV. During experiments,

data were taken at a ring current between 200 and 400 mA. Al metal foil (0.4 μm) was used for initial energy calibration (1559 eV).

A newly designed end station and soft X-ray in-situ cell allows for experiments at atmospheric pressures. The details of the endstation[18,19] and the in situ cell[20] are discussed elsewhere. Samples for transmission experiments were prepared by pressing self-supporting pellets. A sufficient quantity of each sample was used to give an absorbance ($\mu_m \rho x$) between 1.5 and 3.0 calculated[21] at +20 eV above the absorption edge.[16] Typically 7−10 mg of zeolite sample was pressed into a 20 mm diameter (2.2−3.2 mg cm^{-2}) pellet at 15 000 psi.

The intensity of the beam was measured over a 300 eV range (1500 to 1850 eV). An energy step of 0.5 eV was used, and 5 points were averaged at each energy step. A single scan could be completed in 5 min with very high signal-to-noise ratio. All data were checked for reproducibility. Each file contained an I_0 reading measured as the drain current from the M3 mirror under vacuum. Since the mirror contained traces of Si, the Si K-edge at 1839 eV was used for internal calibration of the data.

A portable flow manifold was used to treat the catalysts on-site.[20] Samples of NH_4−Y and Cu−Y were first treated in He (99.999%) flowing at 5 cm^3 min^{-1}. The temperature was increased in increments of 15 K to 673 K for NH_4−Y and 523 K for Cu−Y and maintained at each temperature for the time it took to acquire one scan (5 min). Following conversion of NH_4−Y to H−Y at 673 K, the sample was cooled to room temperature and exposed to ambient atmosphere, after which a final scan was taken.

2.3.3 XAS Analyses. XANES analyses for both Cu K-edge and Al K-edge data have been discussed in detail elsewhere.[22,23] Preedge absorptions due to the background and detector were subtracted using a linear fit to the data in the range of −200 eV to −50 eV relative to the sample edge energy (E_0) for Cu K-edge data and in the range of −150 eV to −20 eV relative to the sample edge energy (E_0) for Al K-edge data. Each spectrum was then normalized by a constant determined by the average absorption in the range of 100 eV to 300 eV relative to E_0 for Cu K-edge data and in the range of 90 eV to 250 eV relative to E_0 for Al K-edge data. The edge-energy of each sample and reference was taken at the first inflection point beyond any preedge peaks.

EXAFS analyses for both Cu K-edge and Al K-edge data have been discussed elsewhere.[22,23] For both data sets, the UWXAFS[24] suite of software programs and its GUI-based equivalent, IFEFFIT[25] were used for analysis. Particular attention was given to the extraction of the $\chi(k)$ function using the AUTOBK background fitting algorithm.[26] For Cu K-edge data, the AUTOBK[26] algorithm was used to select spline points between a k of 1.5 and 15 Å^{-1}, and an R_{bkg} value of 1.0 was chosen. Because the Al K-edge EXAFS information is limited by the Si K-edge at 1839 eV, a background function was subtracted from the normalized data by taking spline points between a k of 0.5 Å^{-1} and 8.36 Å^{-1}. A strong spline clamp was made to the point at 8.36 Å^{-1} and an R_{bkg} value of 1.0 was chosen.

Both Cu K-edge and Al K-edge EXAFS data were fit using FEFF 8.2[27,28] generated scattering paths. For Cu K-edge data, theoretical amplitude and phase functions were calculated for all Cu−O, Cu−Cu, and Cu−Si(Al) coordination environments using scattering paths obtained from atomic coordinates of Cu−metal, CuO, and $[CuOSi(O^tBu)_3]_4$ as reported in earlier studies.[22,29] Additionally, FEFF 8.2 generated scattering paths were calculated for a Cu^+ cation in the site I′, II, and III′ positions using optimized positions from DFT calculations described below. Relevant scattering contributions for all standards were considered initially, but final fits were determined using the following: Cu foil for Cu−Cu interactions, CuO for Cu−O and Cu−Cu interactions, $[CuOSi(O^tBu)_3]_4$ for Cu−Si interactions, and site II for Cu−Al interactions unless otherwise stated. For Al K-edge data, theoretical amplitude and phase functions were calculated for all Al−O, Al−Si, and Al−Cu coordination environments using scattering paths obtained from site I′, II, and III′ positions using optimized position from DFT calculations discussed below. Final fits were determined using site II for Al−O backscattering, however, fits from all Al−O first shell scatters from each site converged to the same value. All FEFF paths were calculated considering self-consistent potentials (Hedin−Lundqvist), $\sigma^2 = 0$, and $S_0^2 = 1$. The generated spectra were referenced to the threshold Fermi level with a reported error of ca. 1 eV using self-consistent calculations.[30]

All fits to Cu K-edge data of Cu−Y samples on the real and imaginary parts of the FT $k^3\chi(k)$ data to magnify the presence of Cu which has its largest backscattering amplitude at high k.[16] FT $k^1\chi$ (k) data were used in the fits to all Al K-edge data. Cu K-edge data were fit between 1.0 and 3.0 Å in R-space following FT between 2.5 and 12.5 Å^{-1}. Al K-edge data were fit in R-space between 0.5 Å and 1.95 Å following FT between 2.25 and 7.5 Å^{-1} with a Hanning window function and a windowsill (dk) of 1 Å^{-1}. Other details of the these fitting approaches can be followed elsewhere.[22,29,31]

In the analysis of Al−Cu scattering from Al K-edge data, a FEFF 8.2 model of Cu at the zeolite exchange site was simulated. The simulation set four Al−O and four Al−Si distances at positions fixed at 1.67 Å and 3.07 Å, respectively. An E_0 shift was set to −12 eV, and σ^2 was set to 0.001 Å^2 for Al−O and Al−Cu paths. Al−Si paths were simulated with a σ^2 set to 0.01 Å^2. To follow the effect of Al−Cu scattering distance, a systematic variation from 2.71 to 2.89 Å was made, as done in previous work.[23]

2.4. Mass Spectrometry. The products formed during vapor-phase exchange of H−Y with CuCl were studied by mass spectrometry. The mass spectrometer was calibrated for H_2 (2 amu), H_2O (18 amu), and HCl (35 amu), the products observed during exchange, using either predefined standards or in-situ reduction of copper standards. CuO and CuCl were used for quantification of H_2O and HCl signals, respectively. These standards were reduced in a 30 cm^3 min^{-1} flow of 0.05 atm H_2 while the temperature was increased at 10 K min^{-1} to 873 K. For the study of the Cu−Y preparation, a 100 mg sample of a CuCl/H−Y physical mixture was used. This physical mixture was the same used to make the full catalyst as described above. 50 cm^3 min^{-1} flow of He was used and an identical temperature program was used as described in the preparation of the bulk catalyst above. For the H_2-TPR measurement, the in-situ prepared Cu^+−Y was cooled to RT and introduced to a total flow of 30 cm^3 min^{-1} of 5% H_2 in He. The temperature was ramped from 298 to 1273 K at 10 K min^{-1}. H_2 (2 amu), H_2O (18 amu), and HCl (35 amu) were measured at a rate of 0.2 samples s^{-1}.

2.5. Catalysts Performance Studies. Details of the experimental setup and data acquisition can be followed elsewhere.[31] 150 mg of catalyst (typically 1.2 cm^3) was loaded into a 10 mm diameter tubular flow reactor made of quartz. Each catalyst was pretreated at 873 K for 1 h in a stream of high purity He (99.999%). For the catalytic experiment, a CO/O_2 mix (25.0% CO, 2.5% O_2, bal He) and He (99.999%) were used. Methanol (CH_3OH) was introduced by passing a CO/O_2 mixture through

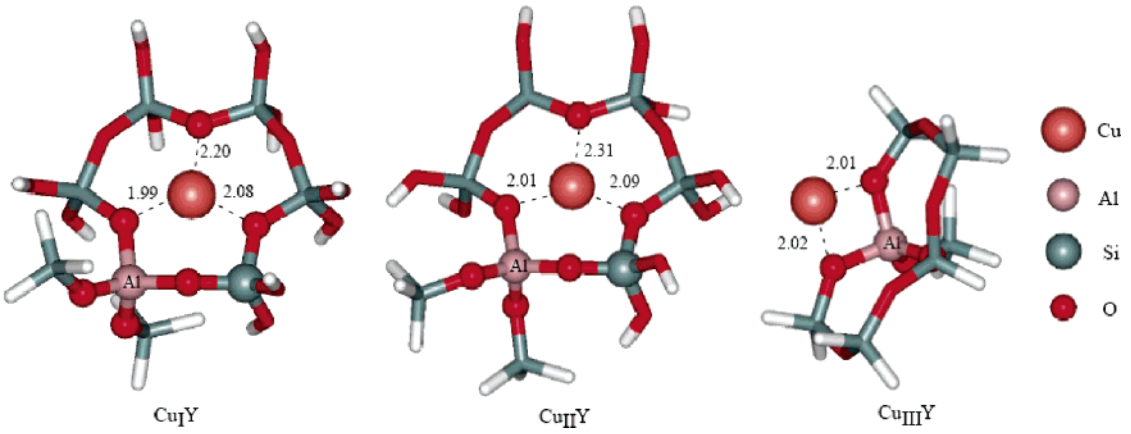

Figure 2. Cluster models calculated by DFT. Cations in sites I′, II′ and III′ are referred to as Cu_IY, $Cu_{II}Y$, and $Cu_{III}Y$, respectively.

a saturator maintained at a constant temperature of 293 K. A $CH_3OH/O_2/CO/He$ mixture (4.0:1.0:9.0:19.3) was fed to the reactor at a nominal total flow rate of 20 $cm^3\ min^{-1}$ and varied between 4 and 40 $cm^3\ min^{-1}$ to study the effect of residence time on product distribution. The feed gas was passed over the catalyst for 45 min. at each respective residence time studied at 403 K. A second experiment designed to study the effect of temperature on the DMC reaction was also carried out on a new Cu−Y sample. For this study, a $CH_3OH/O_2/CO/He$ mixture (4.0:1.0:9.0:19.3) was fed to the reactor at a nominal total flow rate of 20 $cm^3\ min^{-1}$ while the reactor temperature was increased from 298 to 423 K. Two or three points were taken at each temperature (45−60 min). The DMC selectivity is reported on the basis of methanol consumption (S_{DMC/CH_3OH}) and on the basis of CO consumption ($S_{DMC/CO}$). The CO_2 formed is attributed exclusively to CO oxidation, since over the temperature range investigated no evidence was found for the combustion of methanol or products derived from methanol.

2.6. In-Situ FTIR. 7−10 mg of zeolite sample was pressed into a 20 mm diameter (2.2−3.2 mg cm^{-2}) pellet at 15,000 psi. These pellets were loaded into the same microfabricated in-situ cell[20] used for soft X-ray experiments; however, 200 nm thick Si_3N_4 windows (2 mm × 2 mm) were used to provide a stronger and larger transmission area than was used for soft X-ray experiments. Si_3N_4 has an IR transmission window that extends to the limit of the available IR source (550 cm^{-1}). Because catalyst pretreatments and DMC reaction conditions can produce water, conventional windows such as KBr and NaCl were avoided.

Approximately 2−4 mg of Cu−Y was activated in He at 523 K. The temperature was reduced to 403 K to introduce CO/O_2 (0.2 atm CO, 0.02 atm O_2) to the cell. The gas mixture was then saturated by CH_3OH at 298 K and introduced to the cell. All flow rates were approximately 1−2 $cm^3\ min^{-1}$ calibrated to the pressure drop through the microfluidic channels. A detailed description of the gas flow manifold and acquisition system can found elsewhere.[20] All described FTIR measurements of zeolite samples were conducted using a Thermo-Nicolet NEXUS 670 spectrometer. 32 scans were averaged using 2 cm^{-1} resolution.

2.7. Simulation of Cu^+ Siting in Cu−Y. Density functional theory (DFT) was used to predict the coordination and local geometry for Cu^+ cations located in charge-exchange sites I′, II, or III′ of faujasite. Each charge-exchange site was represented by a 25 to 43-atom cluster with the initial atom positions for all Si (Al) and O atoms taken to be those for siliceous faujasite.[32] Each cluster contains one Al and one Cu atom, and is terminated by hydrogen atoms replacing the next oxygen or silicon atom located at the perimeter of the cluster. The hydrogen bond is positioned along the corresponding O−Si bond vector with the resulting O−H bond set to 1.0 Å or along the Si−O bond vector, with the resulting Si−H spacing set to 1.5 Å. The influence of the zeolite lattice was approximated by constraining the terminal H atoms to their initial positions. All remaining atoms were fully relaxed during the electronic structure calculations.

Quantum chemical calculation of the geometries were performed using nonlocal, gradient-corrected density-functional theory (DFT)[33] implemented in Gaussian 98.[34] Becke's three-parameter exchange functional and the correlation functional of Lee, Yang, and Parr (B3LYP) were used to represent the effects of exchange and correlation.[35,36] A mixed basis set has been used: 6-31G** on Al, Si, O, and the acidic proton and the STO-3G basis set on the H atoms terminating the cluster. The 6-311G** Wachters basis set was used for Cu, as suggested in recent theoretical studies of Cu-exchanged zeolite.[37] The models representing the optimized geometries for Cu exchanged in sites I′, II, and III′ of faujasite are referred to as Cu_IY, $Cu_{II}Y$ and $Cu_{III}Y$, respectively.

3. Results and Discussion

3.1. Simulations of Cu^+ Siting in Faujasite. The optimized cluster geometries for Cu^+ cations in the site I′, II, and III′ positions are illustrated in Figure 2. Distances of nearest neighbor oxygen atoms are shown for each cluster. Cu^+ in Cu_IY and $Cu_{II}Y$ is located just above the plane of their respective six-membered O-ring. Bond distances for nearest-neighbor O atoms and next-nearest-neighbor Si and Al atoms are listed in Table 1. The geometries for Cu_IY and $Cu_{II}Y$ are very similar, and for these models Cu^+ is located on average ∼3.1 Å from the Al and Si atoms. The average length of the Al−O bonds to the Cu^+ cation is ∼1.75 Å in both Cu_IY and $Cu_{II}Y$. In contrast to Cu_IY and $Cu_{II}Y$, Cu^+ in $Cu_{III}Y$ is highly coordinatively unsaturated. The cation sits nearly symmetrically at the cation-exchange site. The Cu−O distance is ∼2.01 Å and the Cu−Al distance is 2.69 Å. The Si atoms reside at an average distance of 3.4 Å from the Cu^+ cation.

Cluster calculations for Cu^+-exchanged faujasite have not been reported previously; however, a number of cluster calculations have been made for Cu^+−ZSM-5 and Cu^{2+}−faujasite. Of particular interest to the present work is the Cu−Al separation. Berthomeau et al.[37b] have reported Cu−Al distances in the range of 2.7−2.9 Å for Cu^{2+} exchanged at site II and III positions of faujasite, and Rice et al.[38] have reported a Cu−Al distances of 2.79 Å for Cu^+ exchanged at the T12 site of ZSM-5. Therefore, theoretical calculations have predicted a narrow range of Cu−Al separations.

TABLE 1: Bond Distances Determined from DFT Simulation of Cu Sites

	bond lengths (Å)			
model site	Cu−O	Cu−Al	Cu−Si	Al−O
Cu_IY	1.99	3.04	3.10	1.85
	2.08		3.17	1.77
	2.20		3.21	1.70
	2.82		3.27	1.71
			3.28	
$Cu_{II}Y$	2.01	2.95	3.13	1.84
	2.09		3.19	1.78
	2.31		3.21	1.72
	2.85		3.28	1.73
			3.35	
$Cu_{III}Y$	2.01	2.69	3.36	1.798
	2.02		3.44	1.811
				1.692
				1.726

3.2. Preparation and Site Occupancy of Cu−Y. Based on elemental analysis, Cu−Y contains 23.5 wt. % Cu, 1.1 wt. % Cl, and a trace amount of Na. No Al was removed during high-temperature exchange, and, consequently, the final Si/Al ratio remained unchanged at 2.6. The total Cu/Al ratio was 1.1; however, assuming Cl to be associated with occluded CuCl, the corrected Cu/Al ratio would be 1.0. The presence of CuCl is evidenced by a very small 111 diffraction peak for CuCl in the XRD pattern of Cu−Y. The presence of occluded CuCl has also been observed by Cl K-edge XANES in Cu−USY prepared in a manner similar to that used in this study.[23] Thus, the unit cell formula of the Cu−Y can be written as $[Cu_{54.2}Na_{0.3}Al_{52.8}Si_{139.2}O_{278.4}]$.

Preparation of the Cu−Y by vapor-phase exchange of H−Y with CuCl required handling of H−Y in the absence of water vapor. Moreover, once exposed to water vapor, hydrated H−Y cannot be dehydrated without a loss in the crystallinity of the zeolite.[39] To avoid working with H−Y, it has been suggested that Cu−Y can be produced by vapor phase exchange of NH_4−Y,[7] and, therefore, this approach was explored briefly. It was observed that while vapors of NH_4Cl are formed during exchange, this product decomposes to form NH_3 and HCl, and the NH_3 decomposes above 723 K to form H_2 and N_2. The presence of NH_3 and H_2 contributes to the partial reduction of the exchanged Cu^+ to metallic Cu. Moreover, at lower temperatures, NH_3 forms strong adducts with Cu^+ cations, which cannot be removed.

The preparation of the Cu−Y by high-temperature exchange of dry H−Y with CuCl was monitored by mass spectroscopy. Figure 3 shows the rate of HCl production as a function of time and temperature. As shown in this figure, 0.98 HCl/Cu is formed over the temperature range of the experiment. This stoichiometric ratio supports the expected reaction of CuCl vapor with bridging hydroxyl groups, as illustrated for the site III′ position in the inset of Figure 3, and leads to the conclusion that all of the Cu should be present as Cu^+. A small quantity of H_2O was also released during the reaction of CuCl vapor with the zeolite. This product may have resulted from inadvertent exposure of the zeolite to ambient conditions upon transfer from the N_2-purged drybox to the reactor.

Cu cation positions were initially inferred from the FTIR and XRD data shown in Figures 4 and 5, respectively. Figure 4 compares the infrared spectra for the hydroxyl stretching region of in-situ-prepared H−Y and Cu−Y that had been activated in He at 673 K following exposure to ambient air. H−Y has two well-defined hydroxyl stretches at 3640 and 3540 cm^{-1}, which are attributable to the O−H stretching vibrations of bridging

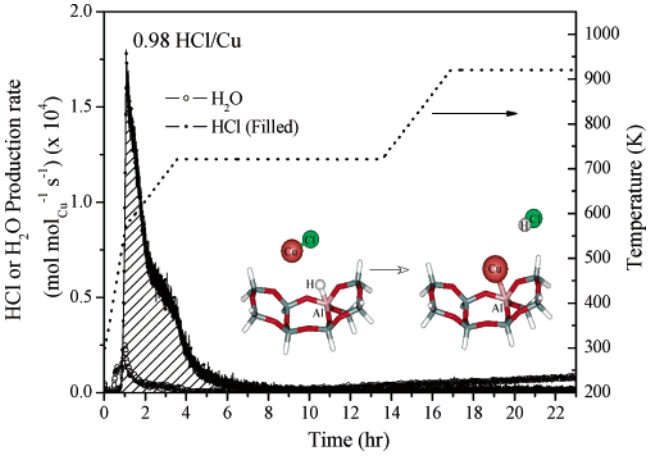

Figure 3. Rates of HCl and H_2O formation during the reaction of H−Y with CuCl.

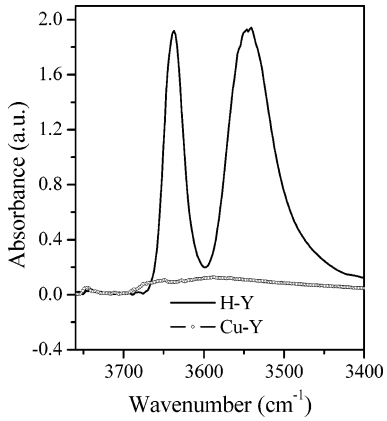

Figure 4. Infrared spectra of the OH stretching region of H−Y and Cu−Y.

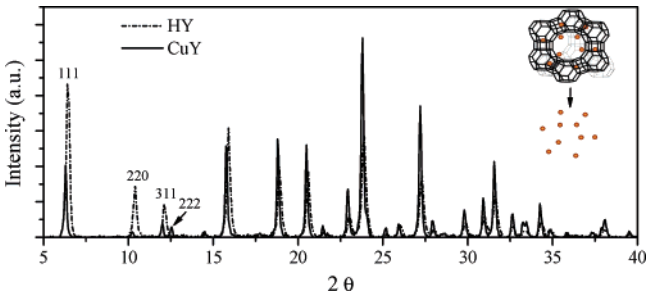

Figure 5. XRD patterns of H−Y and Cu−Y. The inset shows primary lattice of faujasite and the secondary lattice comprised of the Cu cations.

hydroxyls in the supercage and sodalite cage, respectively.[40,41] Both hydroxyl stretches disappeared after the zeolite was exchanged with CuCl, suggesting that the Brønsted acid protons were replaced quantitatively by Cu^+ cations. Figure 5 shows a comparison of the XRD pattern of H−Y and Cu−Y in the hydrated state. The Cu−Y pattern shows a noticeable decrease in intensity of the 111, 220, and 311 diffraction lines at 6.4°, 10.4°, and 12.1°, respectively. The 222 peak at 12.5° becomes visible and diffraction lines at higher angles become more intense. These changes may be a consequence of diffraction from a secondary copper lattice as illustrated in the inset of the figure. It should be noted that, in order for the Cu cations to form a secondary lattice, the zeolite framework Al atoms must be distributed in an ordered fashion. While there is no evidence known for ordering of the Al atoms in Y zeolite, recent ^{27}Al MQ MAS NMR measurements have suggested that the distribution of Al in zeolites, such as zeolite Beta, are not random.[42]

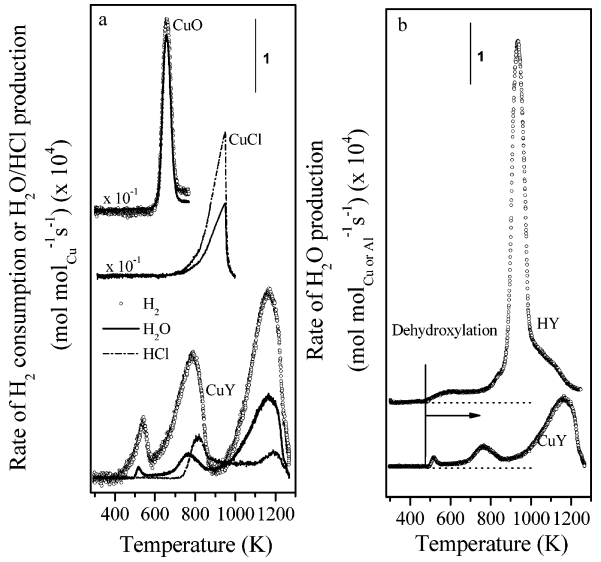

Figure 6. (a) H_2 TPR spectra for CuO, CuCl, and CuY. H_2 consumption and HCl and H_2O production rates are shown for each material. (b) Rate of H_2O production during H_2 TPR of H−Y and Cu−Y.

TABLE 2: H_2 Consumption and Product Formation Observed during H_2 TPR

catalyst	detected gas (x)	*x*/Cu (temp, K) peak 1	peak 2	peak 3	total (*x*/Cu)
CuY	H_2	0.03 (533)	0.15 (783)	0.29 (1163)	0.47
	H_2O	0.003 (518)	0.025 (773)	0.12 (1163)	0.15
	HCl	0.04 (817)	0.04 (1193)		0.10

Direct evidence for the occupation of Cu^+ cations in specific sites associated with the faujasite lattice was obtained from H_2-TPR (Figure 6). Figure 6a shows the rate of H_2 consumption and H_2O and or HCl production for CuO, CuCl, and Cu−Y. The integrated signals for H_2, H_2O, and HCl obtained for both CuO and CuCl are in full agreement with the stoichiometries expected from reactions 1 and 2.

$$H_2 + Cu(II)O \rightarrow Cu(0) + H_2O \quad H_2O/H_2 = 1 \qquad (1)$$

$$^1/_2H_2 + Cu(I)Cl \rightarrow Cu(0) + HCl \quad HCl/H_2 = 2 \qquad (2)$$

The TPR spectrum of Cu−Y shows three H_2 consumption peaks centered at 533, 783, and 1163 K, respectively. The amount of H_2 consumed in each of these peaks is listed in Table 2. The sum of H_2 consumed in each reduction peak is 0.47 H_2/Cu. This is the expected stoichiometry for a one-electron reduction of Cu^+ to metallic Cu. A small quantity of HCl was detected above 813 K (0.10 HCl/Cu). This quantity is consistent with that measured by elemental analysis (0.08 Cl/Cu) and suggests that the release of HCl is due to the reduction of occluded CuCl. H_2O is produced with each H_2 consumption peak. This is surprising since the catalyst had not been exposed to oxygen during preparation. A study of dehydroxylation of H−Y (Figure 6b) suggests that H_2O is produced at temperatures as low as 473 K. The release of H_2O is believed to be associated with the reduction of Cu^+ to metallic Cu. During this process bridging hydroxyl groups are reformed, which can condense immediately if they occur on adjacent or nearby cation-exchange sites. The reformation of bridging hydroxyls by H_2 reduction has been observed in FTIR studies of the Cu−Y prepared by conventional ion exchange.[43] Dehydroxylation results in complete destruction of the zeolite lattice after heating to 1273 K.

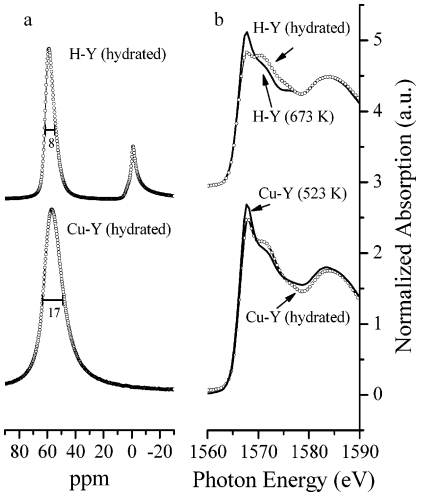

Figure 7. (a) Al^{27} MAS NMR spectra of hydrated H−Y and Cu−Y. (b) Al K-edge XANES of in-situ-prepared H−Y, H−Y hydrated at 298 K, and Cu−Y hydrated at 298 K and after heating to 523 K in He.

The three H_2 TPR peaks seen in Figure 6 for Cu−Y can be assigned to Cu^+ reduction at sites I′, II and III′, as illustrated in Figure 1. Peak 1, centered at 533 K, is assigned to the most accessible position, site III′. Peaks 2 (783 K) and peak 3 (1163 K) are assigned to reduction of Cu^+ cations associated with sites II and I′, respectively. Therefore, 3.4 Cu/unit cell (u.c.) occupy site III′, while 17.2 and 33.3 Cu/u.c. occupy site II and I′, respectively. Rietveld refinement and neutron scattering experiments carried out on Cu^{2+}- and Cu^+-exchanged faujasite have shown that site I or I′ is populated preferentially.[10,11] This site offers the most favorable shielding and sterics for low valence cations.[7] Sites II and II′ are the second most occupied positions for Cu^{2+} cations introduced into Y zeolite by aqueous exchange.[10,11] XRD studies have shown that site III can be occupied by as many as four Cu/u.c.[10] There are no known H_2-TPR studies of Cu−Y prepared by vapor-phase exchange with CuCl. While H_2-TPR spectra of Cu^{2+}-exchanged Y have been reported, the assignments of the reduction peaks have been attributed only to general locations described as sodalite, supercage and hexagonal positions.[13,14]

3.3. Al and Cu K-Edge XAS Characterization of Cu−Y. The coordination of Al in H−Y and Cu−Y was studied by both ^{27}Al MAS NMR and Al K-edge XANES (Figure 7). Figure 7a shows ^{27}Al MAS NMR spectra for H−Y and Cu−Y taken in the hydrated state in order to remove the effects of quadrupolar line broadening.[44] The spectrum of hydrated H−Y shows two lines located at 60 and 0 ppm, which can be assigned to tetrahedrally and octahedrally coordinated Al, respectively.[45−47] Recent studies have revealed that the octahedrally coordinated Al is formed via the reaction of water vapor with the Brønsted acid protons associated with the tetrahedrally coordinated Al,[23,48] as shown in Scheme 1. When the Brønsted acid protons are exchanged by Cu^+ cations, the ^{27}Al NMR peak at 60 ppm broadens and the peak at 0 ppm disappears. The first of these effects is associated with the presence of paramagnetic species,[49] e.g., Cu^+, O_2, whereas the second effect is due to the significantly reduced interaction of Cu^+ cations with water as compared to protons.[38]

The Al K-edge XANES spectra presented in Figure 7b are consistent with the ^{27}Al MAS NMR spectra presented in Figure 7a. Two peaks are observed at 1568 and 1581 eV, which are assigned to Al in tetrahedral and octahedral coordination.[50−53] The XANES spectrum of hydrated H−Y shows evidence for both peaks, but when the sample is dehydrated at 673 K, the

SCHEME 1

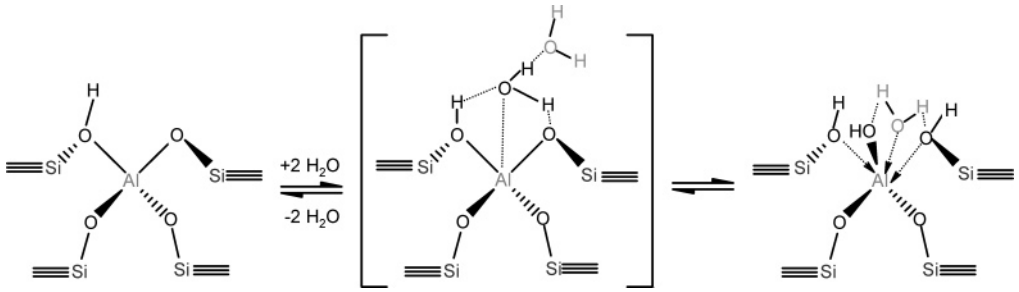

TABLE 3: Peak Energies Observed in Cu K-edge XANES

gas treatment	temp (K)	1s→4p$_{x,y}$[a] (eV)	1s→4p[b] (eV)	1s→3d[c] (eV)
He	673	8983.1	8994.5	
MeOH/He	298, 363, 403	8982.8	8993.9	
CO/He	298, 363, 403[d]	8981.1/8983.3	8994.6	
MeOH/CO/O_2	298	8981.1/8983.3	8993.4	8978.4
	363	8981.1/8983.0	8992.8	8978.1
	403	8981.1/8982.7	8992.2	8977.8

[a] Peak energy in normalized first derivative spectrum. [b] Peak energy in normalized first derivative spectrum associated with highest energy adsorption in the white line. [c] Weak pre-edge peak associated with Cu^{2+} defined at the point of peak inflection. [d] Peak at 8982.0 eV forming.

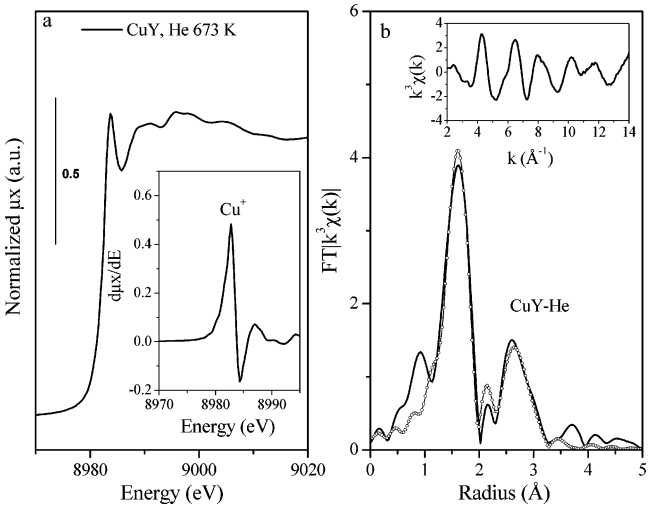

Figure 8. (a) Normalized XANES spectrum of Cu−Y after treatment in He. The inset shows normalized first derivative spectrum. (b) $k^3\chi(k)$ and $FT|k^3\chi(k)|$ of Cu−Y after He pretreatment. $FT|k^3\chi(k)|$ of Cu−Y is shown with best fit in R-space. Original $k^3\chi(k)$ data is shown in the inset.

intensity of the peak for tetrahedrally coordinated Al increases and that for octahedrally coordinated Al decreases, consistent with what is expected on the basis of Scheme 1. Cu−Y in the hydrated state exhibits a greater proportion of tetrahedrally coordinated Al and a somewhat smaller change in the spectrum upon dehydration. These patterns are qualitatively consistent with what has been reported recently for H−USY and Cu−USY, and for H−ZSM-5 and Cu−ZSM-5.[23]

The oxidation state and local structure of Cu in as-prepared Cu−Y was studied using Cu K-edge XAS. Figure 8 shows results for both Cu K-edge XANES and EXAFS. Edge energies (E_0) and characteristic electronic transitions are summarized in Table 3. A prominent edge peak is seen at 8983.7 eV for Cu−Y heated to 673 K in He (Figure 8a). This feature is characteristic of coordinatively unsaturated Cu^+ cations.[54] A similar XANES spectrum has been reported for Cu−Y prepared by vapor-phase exchange of NH_4−Y with CuCl;[7] however, the intensity of the edge peak is half of that seen in the present work. This difference is attributed to the presence of some Cu^+−NH_3 adducts resulting from the preparation procedure which would increase the Cu coordination.

The Fourier transform of $k^3\chi(k)$ for Cu−Y, shown in Figure 8b, exhibits two primary peaks at 1.6 Å and 2.9 Å. The first peak is due to backscattering from O atoms in nearest neighbor positions, and the second peak could result from backscattering from nearest neighbors Si or Al atoms. The data in Figure 8b were fitted in two ways, and the results of both fits are reported in Table 4. In the first case only Cu−O and Cu−Si(Al) shells were considered. This set of assumptions leads to a Cu−O coordination number of about 2 and a value of $R_{Cu-O} = 1.99$ Å, and to a Cu−Si(Al) coordination number of 1 and a value of $R_{Cu-Si(Al)} = 3.12$ Å. While the fit to the experimental data is not bad, a superior fit could be achieved by introducing the effects of backscattering from Cl atoms. From elemental analysis and quantification of the H_2-TPR spectrum of Cu−Y, it was found that approximately 0.10 Cl/Cu are retained in the zeolite, and therefore the coordination number for Cu−Cl backscattering was set at 0.1. The results for the second set of assumptions (see Table 4) leads to a 2-fold improvement in the quality of the fit to the data and to a more physically realistic value of the Cu−Si(Al) coordination number, 2.0. At the same time the values of the CN_{Cu-O}, R_{Cu-O}, and $R_{Cu-Si(Al)}$ remain essentially unchanged relative to the values obtained for the first set of assumptions. The values of R_{Cu-O}, and $R_{Cu-Si(Al)}$ are physically realistic when compared with values for these parameters expected on the basis of DFT calculations (see Table 1). It is also interesting to note that the value of $R_{Cu-Cl} = 2.14$ Å is consistent with a recent EXAFS study of dissolved $[Cl-Cu-Cl]^-$ species in water, which have a Cu−Cl bond distance of 2.13 Å.[55] This observation supports the findings of recent Cl K-edge measurements on Cu−USY prepared by exchange of H−USY with CuCl, which showed evidence for the occlusion of molecularly dispersed CuCl.[23]

Since the analysis of Cu K-edge EXAFS data cannot differentiate between Si and Al backscattering in Cu−Y, Al K-edge EXAFS were taken and analyzed. Figure 9 shows a plot of $k^3\chi(k)$ for as-prepared H−Y and Cu−Y dehydrated at 523 K. The principal difference between H−Y and Cu−Y is observed in the region of 6−8 $Å^{-1}$, the range of wave vectors for which Cu backscattering makes a significant contribution.[16b,23] When Cu^+ cations are exchanged for protons, the peak observed for H−Y splits into two peaks of roughly equivalent intensity. As shown recently, a value of R_{Al-Cu} can be estimated by simulating the k^3-weigthed scattering function, $k^3\chi(k)$.[23] To do so requires estimates of CN_{Al-O} and R_{Al-O}. Values of these parameters were obtained by simulating the peak in the Fourier transform of $k^3\chi(k)$. As seen in Figure 9b, a good agreement could be obtained taking $CN_{Al-O} = 4.0$. The value of R_{Al-O} calculated in this manner is 1.67 Å, which is similar to that

TABLE 4: Parameters Determined from Simulations of EXAFS Data for Cu−Y

method	treatment	shell	N[a]	R (Å)[b]	σ^2 ($\times 10^3$ Å)[c]	ΔE_0 (eV)[d]	R-factor[e]
Cu K-edge	He, 673 K (Fit 1)	Cu−O	1.9 (2)	1.99 (1)	5 (1)	1.2 (1.6)	0.018
		Cu−Si(Al)	1.2 (3)	3.12 (2)			
	He, 673 K (Fit 2)	Cu−O	2.2 (6)	1.98 (2)	7 (3)		
		Cu−Cl	0.1[f]	2.14 (3)	0 (2)	−0.6 (2.2)	0.009
		Cu−Si(Al)	2.0 (1)	3.13 (2)	10 (5)		
Al K-edge	He, 523 K	Al−O	4.2 (6)	1.66 (4)	1[g]	−13.6 (5)	0.072
		Al−Cu[h]	1	2.87			

[a] Coordination number. [b] Fitted radial distance. [c] Debye−Waller factor. [d] Energy reference shift. [e] R-factor. [f] Fixed value based on value determined for Cl/Cu determined by H_2-TPR. [g] Fixed value of $\sigma^2 = 10^{-3}$ [ref 23]. [h] Al−Cu distance was estimated based on FEFF 8.2 model discussed in text.

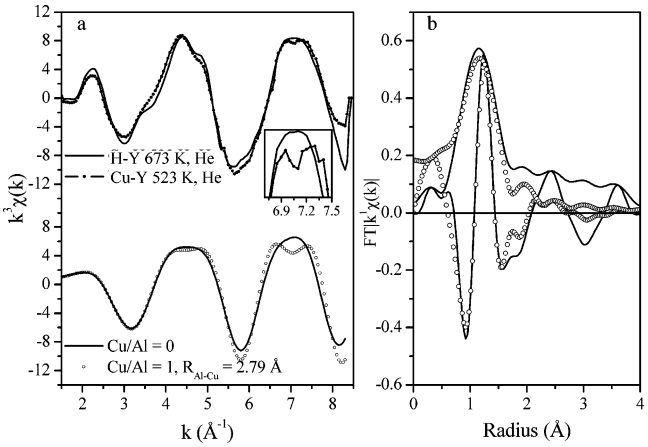

Figure 9. Al K-edge EXAFS of in-situ He-treated Cu−Y. (a) Top half shows $k^3\chi(k)$ data for Cu−Y acquired at 523 K in He, and for H−Y prepared in-situ and acquired at 673 K. Bottom half shows the $k^3\chi(k)$ model data generated by FEFF 8.2, taking Cu/Al = 1 and R_{Cu-Al} = 2.79 Å. (b) $FT|k^1\chi(k)|$ of Cu−Y acquired at 523 K in He and the fit of first Al−O shell (open symbols).

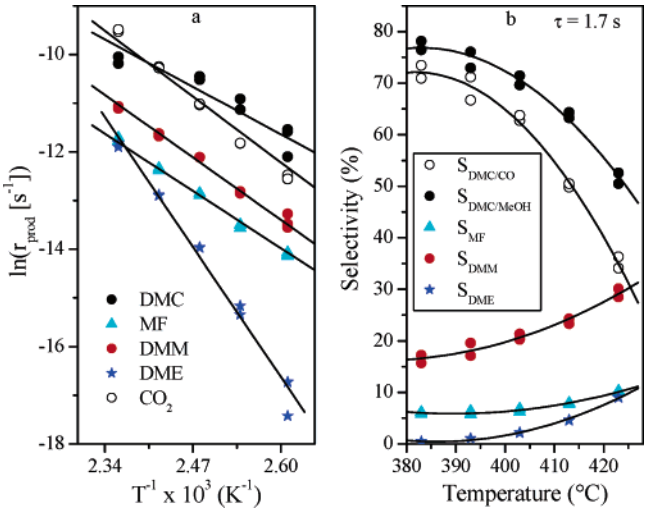

Figure 10. Effects of reaction temperature on (a) the rates of product formation and (b) product selectivity. Feed, CH_3OH(0.12 atm)/CO-(0.20 atm)/O_2(0.02 atm); feed contact time, 1.7s.

reported recently for Cu−USY.[23] Using this value of R_{Al-O} and assuming Cu/Al = 1, based on the results of elemental analysis and the data presented in Figure 3, good qualitative agreement is obtained between the simulated and experimentally observed peak in $k^3\chi(k)$ for the region of 6−8 $Å^{-1}$ is achieved by setting R_{Al-Cu} = 2.79 Å. This value of R_{Al-Cu} is comparable to that estimated from a weighted average of the values determined from DFT calculations (see Table 1), which is R_{Al-Cu} = 2.89 Å. The good agreement between experiment and theory suggests that analysis of Al K-edge EXAFS data for Cu−Y can provide a reasonable estimate for R_{Al-Cu}.

3.4. Measurements of Cu−Y Activity and Selectivity and Characterization of Cu−Y under Reaction Conditions. Experiments were undertaken to determine the activity and selectivity of Cu−Y as a function of reaction temperature at a fixed space velocity and as a function of space velocity at a fixed temperature. The results of the experiments are presented in Figures 10 and 11. With increasing temperature, the rate of formation of each product increases and follows the expected Arrhenius behavior (Figure 10a). Figure 10b shows that with increasing temperature, the selectivity to DMC decreases, whereas that to DMM and MF increases. A small amount of DME is formed even at low temperature, and the selectivity to this product increases slightly with increasing temperature. A very similar pattern is observed (see Figure 11) when the conversion of CH_3OH is varied by decreasing the space velocity (i.e., increasing the residence time) of the feed at a fixed temperature of 403 K. It is also observed that either with increasing reaction temperature or increasing feed residence time, the selectivity of CO consumption to DMC decreases, and consequently the selectivity of CO to CO_2 increases. An estimate of the intrinsic activity of Cu−Y can be made by extrapolating

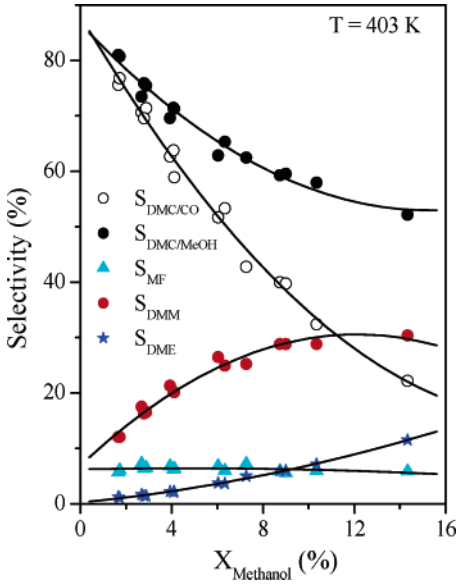

Figure 11. Effect of methanol conversion on product selectivities. Feed, CH_3OH(0.12 atm)/CO(0.20 atm)/O_2(0.02 atm); T = 403 K.

the rate to zero percent conversion. In this limit, the DMC production rate is 5.8×10^{-5} s^{-1} normalized on a total Cu basis and the DMC selectivity with respect to methanol ($S_{DMC/MeOH}$) is 85%. The rate reported for Cu−X at similar reaction conditions is more than half this value;[3] however, earlier reports for Cu−USY are comparable in rate and selectivity.[1]

It is evident from Figure 11 that at very short feed residence times the principal products formed are DMC and water. The changes in product selectivity observed with feed residence time

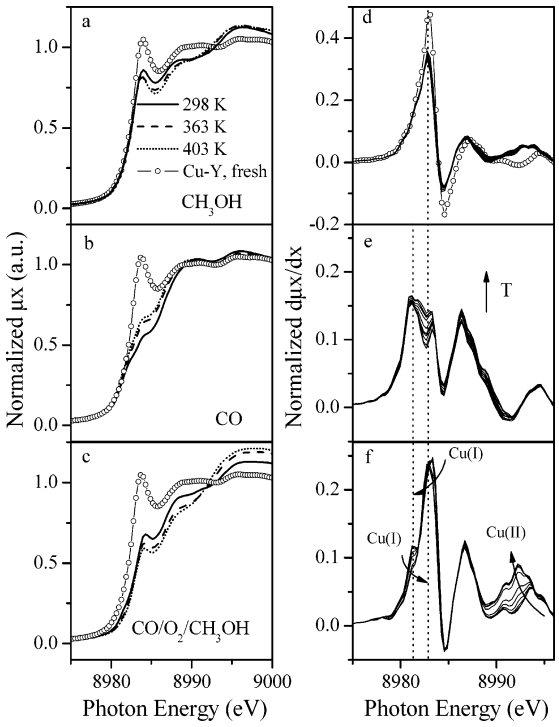

Figure 12. Cu K-edge XANES of Cu−Y under CH_3OH, CO, and DMC reaction conditions. (a), (b), (c) Normalized XANES of Cu−Y exposed to CH_3OH (0.12 atm), CO (0.2 atm), and $CH_3OH/CO/O_2$/ (0.12 atm, 0.2 atm, 0.02 atm), respectively, as the temperature is ramped from 298 to 403 K. The spectra at 298, 363, and 403 K are compared to fresh Cu−Y pretreated in He at 673 K. (d), (e), (f) Normalized derivative spectra for the data in (a), (b) and (c), respectively, detailing the progression of change under all three sets of reaction conditions. Two Cu^+ inflections and one Cu^{2+} inflection are indicated.

can be explained by assuming that H_2O reacts with CO in the feed to produce H_2 and CO_2 via the water gas shift reaction, a reaction which is known to be catalyzed by Cu-containing catalysts.[56] The H_2 produced in this manner might then be expected to hydrogenate the C═O bond of DMC, thereby forming DMM and hydrogenolyze one of the $C(O)-OCH_3$ bonds of DMC to form MF and methanol. The small increase in the selectivity to DME might be attributed to hydrogenolysis of one of the CH_2-OCH_3 bonds of DMM. Such a process seems plausible since Cu−Y does not contain Brønsted acid sites, which are normally required to catalyze the formation of DME from methanol.

Cu K-edge XANES spectra were collected under reaction conditions in order to understand the effects of reactants and reaction temperature on the oxidation state of Cu in Cu−Y. The results are shown in Figure 12 along with similar spectra collected when the catalyst is exposed to CO and CH_3OH alone. The peak positions observed in the normalized derivative spectra are shown in Table 3. Upon contact with CH_3OH, the Cu K-edge XANES feature for Cu^+ cations at 8983.1 eV decreases in intensity slightly, due likely to the interactions of CH_3OH with the Cu^+ cations. Earlier studies have shown evidence from infrared spectroscopy for the formation of methoxy groups and physisorbed methanol when CH_3OH interacts with Cu−X and Cu−USY.[1,3] Such species cause a decrease in intensity of the $1s \rightarrow 4p_{x,y}$ transition seen and a 0.3 eV shift in the first derivative spectrum to 8982.8 eV (Table 3), which is characteristic of an increase in Cu^+ coordination.[54] As the temperature is increased, the position of the $1s \rightarrow 4p_{x,y}$ transition remains constant and there is no further change in the intensity of the transition. The increase in intensity at 8993.9 eV is attributed to multiple scattering processes caused by small changes in the positions of the Cu^+ cations relative to the zeolite lattice.

If CO is absorbed at 298 K on He-treated Cu−Y, the large resonant peak associated with coordinatively unsaturated Cu^+ is replaced by a shoulder at 8984 eV, which is half the intensity seen in He-treated Cu−Y at 673 K. The first derivative spectrum

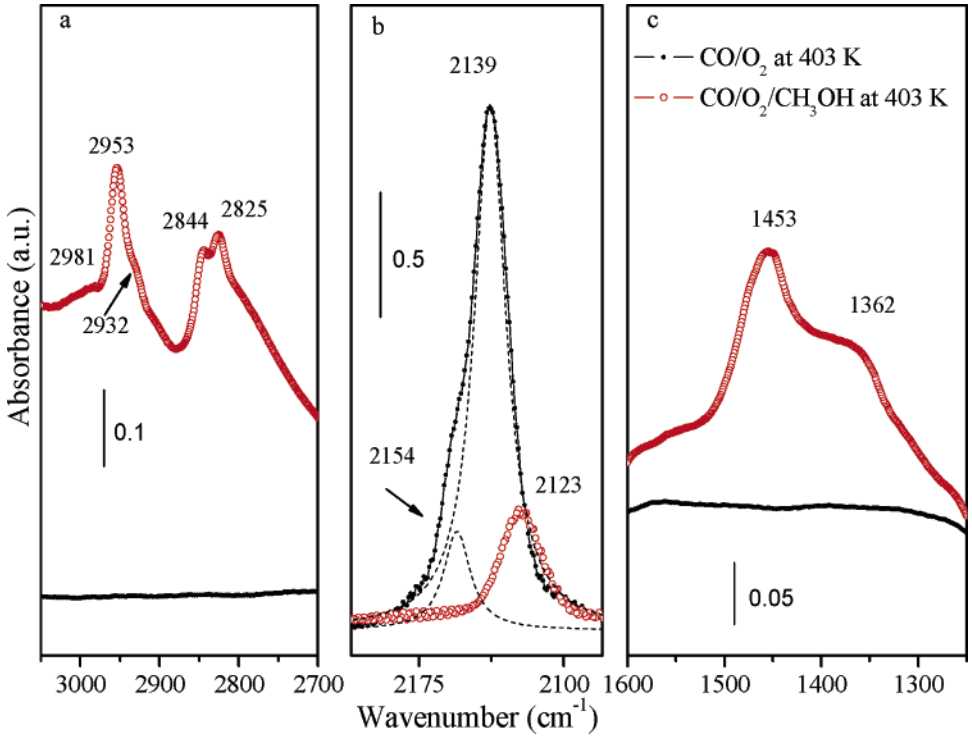

Figure 13. In situ infrared spectra of Cu−Y upon introduction of CO/O_2 (0.2 atm CO, 0.02 atm O_2) and $CH_3OH/CO/O_2$ (0.12 atm CH_3OH, 0.2 atm CO, 0.02 atm O_2) at 403 K. Spectra are referenced to the catalyst spectrum taken at 403 K in He. (a) C−H stretching modes and harmonics of bending modes of methoxide species. (b) CO stretches. Dotted lines shows results of peak deconvolution when the feed is a CO/O_2 mixture (c) Bending modes of methoxide species.

shows two clear peaks at 8981.1 and 8983.3 eV. Oxidation of Cu^+ does not occur in CO, as evidenced by the absence of any change in the intensity of the derivative signal at 8994.5 eV. Therefore, it appears that two types of Cu^+ cations are produced upon exposure of Cu−Y to CO. A similar finding was not reported in previous investigations of CO absorption of either Cu−FAU or Cu−ZSM-5[7,57] but has been noted recently for Cu−ZSM-5.[58] Infrared studies of CO absorption on faujasite suggest that CO cannot penetrate the six-membered O-ring of the sodalite cages,[59,60] and consequently, the peak at 8983.3 eV is assigned to the unperturbed Cu^+ species in site I′. The peak at 8981.1 eV is assigned to the shift in absorption energy caused by the formation of Cu^+−carbonyl species at the sites II and III′.

When Cu−Y is exposed to $CH_3OH/CO/O_2$ at 298 K, the first derivative spectrum again shows two well-defined peaks at 8981.1 and 8983.3 eV in the derivative of the XANES spectrum. The peaks are at the same energies seen as those in the spectrum of CO absorbed on Cu−Y; however, the intensity of the peak at 8983.3 eV is larger. As the temperature is increased from 298 to 403 K, the intensity of the peak at 8981.1 eV decreases while the intensity of the peak at 8983.3 eV shifts to 8982.7 eV. At low temperatures, CO absorption at accessible sites dominates as indicated by the peak at 8981.1 eV. The observed changes can be interpreted as follows. With increasing temperature, Cu^+ sites that contain carbonyls are replaced by methoxy groups. This change is suggested by the shift in the peak from 8983.3 to 8982.7 eV. As noted above, the latter feature is dominant when CH_3OH is adsorbed on Cu−Y. Figure 12f also shows a very small peak near 8978 eV (see Table 3) attributable to the presence of a small concentration of Cu^{2+} cations. The growth in intensity above 8990 eV with increasing reaction temperature seen in the derivative spectra shown in Figure 12f is attributed to changes in the multiple scattering processes caused by changes in the positions of Cu^+ cations relative to the zeolite lattice.

As a complement to the Cu K-edge XANES, in-situ infrared spectra were taken for Cu−Y exposed to CO(0.2 atm)/O_2(0.02 atm) and CH_3OH(0.12 atm)/CO(0.2 atm)/O_2(0.02 atm) at 400 K (Figure 13). For the reaction of excess CO with O_2, the principal feature observed is an intense band at 2139 cm^{-1} with a shoulder at 2154 cm^{-1}. These bands have been observed in previous studies of Cu−Y containing Cu^+ cations and have been assigned to CO absorption on two different types of Cu^+ cations associated to site II.[7] The peak at 2154 cm^{-1} is 13% of the total CO band area. This percentage agrees roughly with the percentage of Cu^+ present in site III′ relative to sites II plus III′, as determined by H_2 TPR. Therefore, the CO stretches at 2154 and 2139 cm^{-1} are assigned to CO absorption on Cu^+ in site III′ and site II, respectively. When CH_3OH is added to the CO/O_2 mixture, the intensity of the bands to adsorbed CO decreases significantly and strong bands appear at 2981, 2953, 2932, 2844, and 2825 cm^{-1}, characteristic of C−H stretching vibrations and harmonics of bending vibrations for methoxide species, and at 1453 and 1362 cm^{-1}, characteristic of bending vibrations for methoxide species and physically adsorbed methanol.[1,3,61] Thus, in agreement with the results obtained from Cu K-edge XANES, in-situ infrared spectroscopy shows that, under reaction conditions, methoxide groups are more strongly bound to Cu^+ cations than to CO. Since the insertion of CO into CH_3O−Cu bonds to form carbomethoxide species has been proposed to be the rate-limiting step in the formation of DMC,[1] it is evident the preferential adsorption of methoxide species relative to CO retards the formation of DMC and must be offset by raising the pressure of CO relative to CH_3OH. Consistent with these observations, it has been reported that the kinetics of DMC formation by oxidative carbonylation of methanol are first order in CO and zero order in CH_3OH.[3] It is also notable that since neither CH_3OH nor CO can access Cu^+ cations bound to sites I, catalysis will occur on those Cu^+ cations bound to sites II and III′.

4. Conclusions

The reaction of H−Y with CuCl vapor leads to the complete exchange of all Brønsted acid protons for Cu^+ cations and only a small occlusion of CuCl. The exchanged Cu^+ cations are located in the site I′, II, and III′ positions within the faujasite structure (see Figure 1). The average Al−O and Al−Cu distances, determined from an analysis of Al K-edge EXAFS data, are 1.67 Å and 2.79 Å, respectively. Analysis of Cu K-edge EXAFS data gives average Cu−O and Cu−Si(Al) distances of 1.99 Å and 3.13 Å, respectively. All of the average distances are consistent with those determined from DFT simulations of Cu^+ exchanged into sites I′, II, and III′. Upon exposure to a feed mixture containing CH_3OH, CO, and O_2, Cu−Y produces DMC, DMM, and MF, as well as a small amount of DME. The primary product observed at very short feed contact times is DMC, and at longer contact times, the selectivity to DMC decreases while those to DMM and DME increase. It is proposed that DMM and DME are formed by the hydrogenation of DMC and the hydrogenolysis of DMM, respectively, the H_2 for these reactions being formed by the reaction of H_2O produced during DMC synthesis with CO in the feed. In-situ Cu K-edge XANES and infrared spectroscopy indicate that the majority of the copper cations remain as Cu^+. Only those copper cations present in sites II and III′ are accessible to reactants, and hence only these cations contribute to the activity of the catalyst. It is also observed that methoxide groups are the dominant adsorbed species and that adsorbed CO is a minority species under reaction conditions.

Acknowledgment. We would like to thank Jason Bronkema and Konstantin Pokrovski for their help in the collection of the XAS data. Portions of this research were carried out at the Stanford Synchrotron Radiation Laboratory, a national user facility operated by Stanford University on behalf of the U.S. Department of Energy, Office of Basic Energy Sciences. We would also like to thank Professor Hisanobu Wakita of the Department of Chemistry, Fukuoka University, Japan, who supported our use of the atmospheric end station at B.L. 6.3.1 of the ALS at the Lawrence Berkeley National Laboratory. This work was supported by the Methane Conversion Cooperative, funded by BP, and in part (TCNL) by the National Institutes of Health (HG01399). Additional support was provided by the Director of the Office of Science, Office of Basic Energy Sciences, Division of Chemical Sciences, Geosciences, and Biosciences and the Division of Materials Sciences of the U.S. Department of Energy at the ALS and LBNL under Contract No. DE-AC02-05CH11231.

References and Notes

(1) (a) King, S. T. *J. Catal.* **1996**, *161*, 530. (b) King, S. T. *Catal. Today* **1997**, *33*, 173.

(2) (a) King, S. T.; Jones, M. E.; Olken, M. M. U.S. Patent 5,391,803, 1995. (b) Molzahn, D. C.; Jones, M. E.; Hartwell, G. E.; Puga, J. U.S. Patent 5,387,708.

(3) (a) Anderson, S. A.; Root, T. W. *J. Catal.* **2003**, *217*, 396. (b) Anderson, S. A.; Root, T. W. *J. Mol. Catal. A* **2004**, *220*, 247.

(4) Pacheco, M. A.; Marshall, C. L. *Energy Fuels* **1997**, *11*, 2.

(5) (a) Herman, R. G.; Lunsford, J. H.; Beyer, H.; Jacobs, P. A.; Uytterhoeven, J. B. *J. Phys. Chem.* **1975**, *79*, 2388. (b) Jacobs, P. A.; Linart, J. P.; Nus, H.; Uytterhoeven, J. B.; Beyer, H. *J. Chem. Soc., Faraday Trans 1* **1977**, *73*, 1745.

(6) Gentry, S. J.; Hurst, N. W.; Jones, A. *J. Chem. Soc., Faraday Trans 1* **1979**, *75*, 1688.

(7) Palomino, G. T.; Bordiga, S.; Zecchina, A.; Marra, G. L.; Lamberti, C. *J. Phys. Chem. B* **2000**, *104*, 8641.

(8) Lamberti, C.; Spoto, G.; Scarano, D.; Pazé, C.; Salvalaggio, M.; Bordiga, S.; Zecchina, A.; Palomino, G. T.; D'Acapito, F. *Chem. Phys. Lett.* **1997**, *269*, 500.

(9) Smith, J. V. *Adv. Chem. Ser.* **1971**, *101*, 171.

(10) Fowkes, A. J.; Ibberson, R. M.; Rosseinsky, M. J. *Chem. Mater.* **2002**, *14*, 590.

(11) Maxwell, I. E.; de Boer, J. J.; Downing, R. S. *J. Catal.* **1980**, *64*, 493.

(12) Hüber, G.; Rauhut, G.; Stoll, H.; Roduner, E. *J. Phys. Chem. B* **2003**, *107*, 8568.

(13) Kieger, S.; Delahay, G.; Coq, B.; Neveu, B. *J. Catal.* **1999**, *183*, 267.

(14) Kieger, S.; Delahay, G.; Coq, B. *Appl. Catal. B* **2000**, *25*, 1.

(15) Jentoft, R. E.; Deutsch, S. E.; Gates, B. C. *Rev. Sci. Instrum.* **1996**, *67*, 2111.

(16) (a) Stern, E. A.; Kim, K. *Phys. Rev. B* **1981**, *23*, 378. (b) Koningsberger, D. C.; Prins, R. *X-ray Absorption*; Wiley: New York, 1988. (c) Koningsberger, D. C.; Mojet, B. L.; van Dorssen, G. E.; Ramaker, D. E. *Top. Catal.* **2000**, *10*, 143. (d) Teo, B. K. *EXAFS: Basic Principles and Data-Analysis*; Springer: New York, 1986.

(17) Underwood, J. H.; Gullikson, E. M. *J. Electron Spectrosc. Relat. Phenom.* **1998**, *92*, 265.

(18) Nachimuthu, P.; Matsuo, S.; Farangis, B.; Lindle, D. W.; Wakita, H.; Perera, R. C. C. *J. Alloys Compd.* **2004**, *362*, 124.

(19) ALS internal communication: http://www-als.lbl.gov/als/compendium. Matsuo, S.; Kurisaki, T.; Yamashige, H.; Nachimuthu, P.; Perera, R. C. C.; Wakita, H. *Development and evaluation of a new liquid cell system for soft X-ray absorption experiments.*

(20) Drake, I.; Liu, C. N.; Gilles, M.; Tyliszczak, T.; Kilcoyne, A. L. D.; Shuh, D.; Mathies, R. A.; Bell, A. T. *Rev. Sci. Instrum.* **2004**, *75*, 3242.

(21) Values were calculated using the web interface of the Center for X-ray Optics at Lawrence Berkeley National Laboratory, Berkeley, CA: http://www-cxro.lbl.gov/optical_constants/pert_form.html.

(22) Drake, I. J.; Fujdala, K. L.; Baxamusa, S.; Bell, A. T.; Tilley, T. D. *J. Phys. Chem. B* **2004**, *108*, 18421.

(23) Drake, I. J.; Zhang, Y.; Gilles, M.; Teris Liu, C. N.; Nachimuthu, P.; Perera, R. C. C.; Wakita, H.; Bell, A. T. *J. Phys. Chem. B* **2006**, *110*, 11665.

(24) (a) Stern, E. A.; Newville, M.; Ravel, B.; Yacoby, Y.; Haskel, D. *Physica B* **1995**, *208*−*209*, 117. (b) Newville, M.; Ravel, B.; Haskel, D.; Rehr, J. J.; Stern, E. A.; Yacoby, Y. *Physica B* **1995**, *208*−*209*, 154.

(25) (a) Newville, M. *J. Synchrotron Radiat.* **2001**, *8*, 322. (b) IFEFFIT manual: http://cars9.uchicago.edu/ifeffit/. (c) Ravel, B.; Newville, M. *Phys. Scr.* **2005**, *T115*, 1007. (d) Ravel, B.; Newville, M. *J. Synchrotron Radiat.* **2005**, *12*, 537.

(26) Newville, M.; Liviò'', P.; Yacoby, Y.; Rehr, J. J.; Stern, E. A. *Phys. Rev. B* **1993**, *47*, 14126.

(27) Ankudinov, A. L.; Rehr, J. J. *Phys. Rev. B* **1997**, *56*, R1712.

(28) Ankudinov, A. L.; Bouldin, C.; Rehr, J. J.; Sims, J.; Hung, H. *Phys. Rev. B* **2002**, *65*, 104107.

(29) Drake, I. J.; Fujdala, K. L.; Bell, A. T.; Tilley, T. D. *J. Am. Chem. Soc.* **2004**, *126*, 10864.

(30) (a) Rehr, J. J.; Albers, R. C. *Rev. Mod. Phys.* **2000**, *72*, 621. (b) Manual for FEFF8: http://feff.phys.washington.edu/feff/.

(31) Drake, I. J.; Fujdala, K. L.; Bell, A. T.; Tilley, T. D. *J. Catal.* **2005**, *230*, 14.

(32) Hriljac, J. J.; Eddy, M. M.; Cheetham, A. K.; Donohue, J. A.; Ray, G. J. *J. Solid State Chem.* **1993**, *106*, 66.

(33) Parr, R. G.; Yang, W. *Density-Functional Theory of Atoms and Molecules*; Oxford University Press: Oxford, 1989.

(34) Frisch, M. J.; Trucks, G. W.; Schlegel, H. B.; Scuseria, G. E.; Robb, M. A.; Cheeseman, J. R.; Zakrzewski, V. G.; Montgomery, J. A., Jr.; Stratmann, R. E.; Burant, J. C.; Dapprich, S.; Millam, J. M.; Daniels, A. D.; Kudin, K. N.; Strain, M. C.; Farkas, O.; Tomasi, J.; Barone, V.; Cossi, M.; Cammi, R.; Mennucci, B.; Pomelli, C.; Adamo, C.; Clifford, S.; Ochterski, J.; Petersson, G. A.; Ayala, P. Y.; Cui, Q.; Morokuma, K.; Malick, D. K.; Rabuck, A. D.; Raghavachari, K.; Foresman, J. B.; Cioslowski, J.; Ortiz, J. V.; Stefanov, B. B.; Liu, G.; Liashenko, A.; Piskorz, P.; Komaromi, I.; Gomperts, R.; Martin, R. L.; Fox, D. J.; Keith, T.; Al-Laham, M. A.; Peng, C. Y.; Nanayakkara, A.; Gonzalez, C.; Challacombe, M.; Gill, P. M. W.; Johnson, B. G.; Chen, W.; Wong, M. W.; Andres, J. L.; Head-Gordon, M.; Replogle, E. S.; Pople, J. A. *Gaussian 98*; Gaussian, Inc.: Pittsburgh, PA, 1998.

(35) Becke, A. D. *Phys. Rev. A* **1988**, *38*, 3098.

(36) Lee, C.; Yang, W.; Parr, R. G. *Phys. Rev. B* **1988**, *37*, 785.

(37) (a) Berthomieu, D.; Ducéré, J. M.; Goursot, A. *J. Phys. Chem. B* **2002**, *106*, 7483. (b) Berthomieu, D.; Krishnamurty, S.; Coq, B.; Delahay, G.; Goursot, A. *J. Phys. Chem. B* **2001**, *105*, 1149.

(38) Rice, M. J.; Chakraborty, A. K.; Bell, A. T. *J. Phys. Chem. A* **1998**, *102*, 7498.

(39) (a) Parker, L. M.; Bibby, D. M.; Burns, G. R. *Zeolites* **1991**, *11*, 293. (b) Breck, D. W. *Zeolite Molecular Sieves*, John Wiley: New York, 1974. (c) Kerr, G. T. *J. Catal.* **1982**, *77*, 307.

(40) Anderson, M. W.; Klinowski, J. *Zeolites* **1986**, *6*, 455.

(41) Eichler, U.; Brändle, M.; Sauer, J. *J. Phys. Chem. B* **1997**, *101*, 10035.

(42) Abraham, A.; Lee, S. H.; Shin, C. H.; Hong, S. B.; Prins, R.; van Bokhoven, J. A. *Phys. Chem. Chem. Phys.* **2004**, *6*, 3031.

(43) Valyon, J.; Hall, W. K. *J. Phys. Chem.* **1993**, *97*, 7054.

(44) Klinowski, J.; Fyfe, C. A.; Gobbi, G. C. *J. Chem. Soc., Faraday Trans. 1* **1985**, *81*, 3003.

(45) (a) Meadows, M. D.; Smith, K. A.; Kinsey, R. A.; Rothgeb, T. M.; Skarjune, R. P.; Oldfield, E. *Proc. Natl. Acad. Sci. U.S.A.* **1982**, *79*, 1351. (b) Mastikhin, V. M.; Krivoruchko, O. P.; Zolotovskii, B. P.; Bayanov, R. A. *React. Kinet. Catal. Lett.* **1981**, *18*, 117. (c) Fyfe, C. A.; Gobbi, C. G.; Hartman, J. S.; Klinowski, J.; Thomas, J. M. *J. Phys. Chem.* **1982**, *86*, 1247.

(46) Klinowski, J.; Thomas, J. M.; Fyfe, C. A.; Gobbi, G. C. *Nature* **1982**, *296*, 533.

(47) Bourgeat-Lami, E.; Massiani, P.; Di Renzp, F.; Espiau, P.; Fajula, F. *Appl. Catal.* **1991**, *72*, 139.

(48) Omega, A.; Prins, R.; van Bokhoven, J. A. *J. Phys. Chem. B* **2005**, *109*, 9280.

(49) Petunchi, J. O.; Marcelin, G.; Hall, W. K. *J. Phys. Chem.* **1992**, *96*, 9967.

(50) Van Bokhoven, J. A.; Sambe, H.; Ramaker, D. E.; Koningsberger, D. C. *J. Phys. Chem. B* **1999**, *103*, 7557.

(51) Shimizu, K.; Kato, K.; Yoshida, T.; Yoshida, H.; Satsuma, A.; Hattori, T. *Chem. Commun.* **1999**, 1681.

(52) McKeown, D. A.; Waychunas, G. A.; Brown, G. E., Jr. *J. Non-Cryst. Solids* **1985**, *74*, 349.

(53) Yoon, T. H.; Johnson, S. B.; Benzerara, K.; Doyle, C. S.; Tyliszczak, T.; Shuh, D. K.; Brown, G. E., Jr. *Langmuir* **2005**, *21*, 5002.

(54) Kau, L. S.; Spira-Solomon, D. J.; Penner-Hahn, J. E.; Hodgson, K. O.; Solomon, E. I. *J. Am. Chem. Soc.* **1987**, *109*, 6433.

(55) Fulton, J. L.; Hoffmann, M. M.; Darab, J. G. *Chem. Phys. Lett.* **2000**, *330*, 300.

(56) Koryabkina, N. A.; Phatak, A. A.; Ruettinger, W. F.; Farrauto, R. J.; Ribeiro, F. H. *J. Catal.* **2003**, *217*, 233.

(57) Bolis, V.; Maggiorini, S.; Meda, L.; D'Acapito, F.; Palomino, G. T.; Bordiga, S.; Lamberti, C. *J. Chem. Phys.* **2000**, *113*, 9248.

(58) Prestipino, C.; Capello, L.; D'Acapito, F.; Lamberti, C. *Phys. Chem. Chem. Phys.* **2005**, *7*, 1743.

(59) Bordiga, S.; Scarano, D.; Spoto, G.; Zecchina, A.; Lamberti, C.; Areán, C. O. *Vibr. Spectrosc.* **1993**, *5*, 69.

(60) Bordiga, S.; Garrone, E.; Lamberti, C.; Zecchina, A.; Areán, C. O.; Kazansky, V. B.; Kustov, L. M. *J. Chem. Soc., Faraday Trans.* **1994**, *90*, 3367.

(61) Forester, T. R.; Howe, R. F. *J. Am. Chem. Soc.* **1987**, *109*, 50 76.